Macromolecular Rapid Communications
www.mrc-journal.de

Supersoft Polymer Melts in Binary Blends of Bottlebrush *cis*-1,4-Polyfarnesene and *cis*-1,4-Polyisoprene

Ioannis Tzourtzouklis, Moritz Meier-Merziger, Holger Frey, and George Floudas**

Binary blends of polyterpenes are employed comprising *cis*-1,4-polyfarnesene (PF) with a bottlebrush architecture, and linear *cis*-1,4-polyisoprene (PI) as model systems toward supersoft polymer melts. The bottlebrush PF results in a low plateau modulus ($G_N^0 \approx 3.5 \times 10^4$ Pa) that can further be reduced with the addition of PI. Depending on the fraction of short PI chains in the *athermal* and nearly *isofrictional* blends, plateau moduli in the range from 1 to 10 kPa can be achieved. Tube dilation is very efficient in the present binary blends as compared to more common blends comprising long/short or linear/star chains of identical polymer structure.

1. Introduction

Biological materials have elastic moduli that range from ≈10 Pa (supersoft tissues) to ≈10^7 Pa (skin and tendons).[1–2] Mimicking soft biological tissues with polymeric materials requires a specific architectural design based on brush-like motifs.[3–6] The underlying idea is that the bottlebrush architecture will increase the diameter of polymer chains, and as a result, dilute the entanglements (i.e., increase the entanglement molar mass, M_e). Linear polymer melts fail this exercise, with M_e in the range from 10^3 to 10^4 g mol^{-1} the rubbery plateau modulus, G_N^0, ($G_N^0 = \frac{4}{5}\frac{\rho RT}{M_e}$, where ρ is the mass density, T is the temperature and R is the Avogadro number) is in the range from 10^5 to 10^6 Pa, i.e., much higher than the one encountered in soft biological tissues. Contrasting this with bottlebrush polymers, scaling arguments predict[7] that the plateau modulus scales with the tube diameter, d_T, and the number of units of the side chains (n_{sc}) as $G_N^0 \sim M_e^{-1} \sim d_T^{-3} \sim n_{sc}^{-3/2}$. In addition to n_{sc}, the mechanical response is controlled by the grafting density (n_g^{-1}), i.e., the number of side chains per backbone repeat unit. In networks made of bottlebrush polymers, another important parameter is the degree of polymerization of the strand backbone (n_x). In this case, the triplet (n_{sc}, n_g, n_x) controls the mechanical response of the network.

Earlier studies[8,3–5] demonstrated that solvent-free polymer melts with the bottlebrush architecture comprising side chains attached to each repeat unit along the backbone, exhibit viscoelastic properties reminiscent of the bare backbone polymer in the presence of a diluent. Subsequent cross-linking of the undiluted bottlebrush polymer resulted in a plateau modulus of ≈1 kPa, a value typically found in networks swollen by a diluent.[8]

Here we employ a different approach toward supersoft polymer melts. It is based on a recent investigation of the viscoelastic and dielectric properties of polymyrcene (PMyr),[9] a bio-based polymer belonging to the class of polyterpenes (other known members are the *cis*-1,4-PI, and the *cis*-1,4-PF[10]). Polyterpenes[11–14] constitute a class of type-A polymers, where by architectural design one can control the "thickness" of chains and henceforth the chain dynamics. As expected, chain thickening greatly affects the viscoelastic properties: In going from PI to PMyr and PF, the entanglement molar mass increases (from 5 kg·mol^{-1} in PI, to 22 kg·mol^{-1} in PMyr, to 50 kg·mol^{-1} in PF). Similarly, the packing length increases (from 3.1 Å in PI to 4.7 Å in PMyr and to 6.3 Å in PF). Lastly, the plateau modulus decreases (from 0.35 MPa in PI, to 0.1 MPa in PMyr, and to 0.035 MPa in PF). Furthermore, the plateau modulus followed the empirical relation: $G_N{}^0 = 0.00226\ k_B T/p^3$ consistent with the proportionality between the tube diameter and the packing length, p.[15,9]

Motivated by the above findings, we employ binary blends of polyterpenes aiming to exert additional control over the plateau modulus and packing and henceforth to trigger the flow behavior. Inherent to the blend studies of long/short chains is the concept of constraint release (CR) of the long chain motions by the shorter chains, the latter acting effectively as a solvent.[16–20] In bidisperse blends with identical chemistry[21–24] comprising entangled long chains (molar mass, M_L, volume

I. Tzourtzouklis, G. Floudas
Department of Physics
University of Ioannina
P.O. Box 1186, Ioannina 45110, Greece
E-mail: gfloudas@uoi.gr
M. Meier-Merziger, H. Frey
Department of Chemistry
Johannes Gutenberg University Mainz
Duesbergweg 10–14, 55128 Mainz, Germany
E-mail: hfrey@uni-mainz.de
G. Floudas
Max Planck Institute for Polymer Research
Ackermannweg 10, 55128 Mainz, Germany
G. Floudas
University Research Center of Ioannina (URCI)-Institute of Materials Science and Computing
Ioannina 45110, Greece

The ORCID identification number(s) for the author(s) of this article can be found under https://doi.org/10.1002/marc.202400551

DOI: 10.1002/marc.202400551

fraction, φ_L) and entangled short chains (molar mass, M_S) the terminal dynamics are determined by the relative relaxation of the repeating long chains, $\tau_{L,rept.} = 3\tau_e(\frac{M_L}{M_e})^3$, versus the CR Rouse relaxation, $\tau_{CR} = 3\tau_e(\frac{M_S}{M_e})^3(\frac{M_L}{M_e})^2$, and the final entanglement density, $Z = (\frac{M_L}{M_e})\ \varphi_L^{\alpha}$, where α is the dilution exponent. In the present case the short/long chains form an *athermal* blend, but the components are not chemically identical, possessing very different M_e values. We show that *athermal* binary PF/PI blends where one component (PF) has a bottlebrush architecture and the other comprises linear chains (PI), constitute a new class of supersoft polymer melts. Depending on the fraction of short PI chains in the blend, plateau moduli as low as 1 kPa could be obtained.

2. Experimental Section

2.1. Synthesis

Synthesis: All polymerizations were made under an inert argon atmosphere as described elsewhere in detail.[12–14,9] β-Farnesene was freed from its stabilizer by passing it through alkaline aluminum oxide. Subsequently, it was dried over calcium hydride for 24 h and degassed using at least three *freeze-pump-thaw* cycles. Then a 25 vol% solution of trioctyl aluminum in cyclohexane was added, and the solvent was removed in vacuo. The solvent *n*-heptane was dried using *sec*-butyl lithium (*s*-BuLi) and 1,1.diphenyl ethylene. Both monomer and solvent were freshly distilled prior to use and transferred into an argon-filled glove box. Polymerizations were carried out at a volume concentration of β-farnesene to *n*-heptane of 1:9 and initiated using the respective amount of *s*-BuLi (1.3 molar solution) for the targeted molar mass ($M_n = M_0 \cdot [M]_0/[I]$); where M_0 = molar mass of β-farnesene, $[M]_0$ = monomer concentration and [I] = initiator concentration). The polymerizations were run over night at either ambient temperature or at 70 °C and terminated with degassed methanol. Thereafter, the reaction mixture was concentrated in vacuo and finally precipitated in isopropyl alcohol/methanol. By centrifugation and decantation, the polymeric material was separated from the solvent mixture. The polymer was redissolved in chloroform and precipitated a second time. The isolated polymer was dissolved in benzene and freeze-dried for at least 72 h at 40 °C in vacuo (1×10^{-3} mbar) to remove any traces of solvents. Approximate quantitative yields of >95% were obtained. The deviation can be attributed to a loss during purification. All samples were characterized via size-exclusion chromatography (SEC) and nuclear magnetic resonance spectroscopy (NMR).

The polyisoprene samples were purchased from *PSS Polymer Standards*, Mainz, Germany. As calibration standards for SEC instruments, they offer analytic purity and certificates, i.e., number average molar mass (M_n), mass average molar mass (M_w), and low dispersity ($Đ$). All values were measured by RI-detection in THF relying on a polyisoprene calibration. In addition, mass average molar mass (M_w^{MALS}) values obtained by multi-angle light scattering (MALS) were given. The molecular characteristics of the PF and PI samples were provided, respectively, in Tables S1 and S2 (Supporting Information).

2.2. Analytic Measurements—Size Exclusion Chromatography (SEC)

All samples were measured using tetrahydrofuran (THF) as eluent and a polyisoprene calibration. A set-up consisting of: Waters 717 plus autosampler, a SpectraSeries-P100 pump, a column set (MZ-Gel SD plus e5/e3/100) of MZ-Analysetechnik, Mainz, an Agilent G1362A RI-Detector, and a MZ-Messanalytik TSP (254 nm) UV-detector were used. SEC traces for the PF homopolymers were shown in Figure S1 (Supporting Information). As for the determination of the absolute molar mass, all samples were additionally measured using a multi-angle light scattering (MALS) detector. For these samples a column set PSS SDV 5 µm pc/ PSS SDV 5 µm 1 000 Å/ PSS SDV 5 µm 100 000 Å/ PSS SDV 5 µm 1 000 000 Å was used. It was measured on an Agilent 1200 setup. The comparison of the molar mass of all PF and PI samples, determined by SEC with MALS detector is shown in Figure S2 (Supporting Information).

2.3. Analytic Measurements—Nuclear Magnetic Resonance Spectroscopy (NMR)

All samples were measured on a 400 MHz Bruker Avance II HD 400 instrument. Spectra (^{1}H, ^{13}C, COSY, and HSQC) were recorded at the maximum frequency for each nucleus (400 MHz for ^{1}H and 101 MHz for ^{13}C). All measured spectra were processed using the software "*MestReNova v14.2.0*" from Mestrelab Research S.L., Santiago de Compostela, Spain. The spectra were normalized to the respective proton signal of the deuterated solvent of choice and phase and baseline corrected. ^{1}H NMR spectra of PF_{17} and PI_{64} are provided in Figures S3 and S4 (Supporting Information), respectively.

2.4. Rheology

The viscoelastic properties of all blends have been studied with the TA Instruments Rheometer AR-G2 equipped with a magnetic bearing that allows for nanotorque control. Measurements were performed in an environmental test chamber (ETC). Samples were prepared on the lower rheometer plate (8 mm), and the upper plate was adjusted aptly to ensure a uniform gap thickness. Temperature control was achieved through a nitrogen convection oven. The linear and non-linear viscoelastic regimes were determined by the strain amplitude dependence of the complex shear modulus $|G^*|$, at $\omega = 10$ rad s^{-1}. Data of the complex shear modulus as a function of frequency were obtained by frequency sweeps in the range of 0.1–100 rad s^{-1} for several temperatures near and above the glass temperature. According to the principle of time–temperature superposition (*t*Ts), the frequency dependence of the complex shear modulus G^* at any temperature can be obtained from a master curve at a reference temperature (here $T_{ref} = 253$ K for all the cases) according to the equation: $G^*(\omega,T) = b_T G^*(a_T\omega,T_{ref})$.

2.5. Dielectric Spectroscopy

Dielectric spectroscopy measurements as a function of temperature (i.e., under "isobaric" conditions) were performed with the

Table 1. Molar mass (M_n), number of entanglements (Z), and composition (w) of the binary bottlebrush/linear PF/PI blends.

BLENDS	Name	M_n^{PI} [g mol^{-1}]	M_n^{PF} [g mol^{-1}]	Z_{PI}	Z_{PF}	w_{PI}	w_{PF}
CASE I	BLD-PI(M$_e$)	4500	129 000	0.9	2.6	0.5	0.5
PF(3M_e) / PI	BLD-PI(2 M$_e$)	9900	129 000	2.0	2.6	0.5	0.5
	BLD-PI(4 M$_e$)	19 000	129 000	3.8	2.6	0.5	0.5
	BLD-PI(8 M$_e$)	38 800	129 000	7.8	2.6	0.5	0.5
	BLD-PI(20 M$_e$)	103 000	129 000	20.6	2.6	0.5	0.5
	BLD-PI(30 M$_e$)	150 000	129 000	30	2.6	0.5	0.5
CASE II	BLD-PF(3 M$_e$)	4500	129 000	0.9	2.6	0.5	0.5
PI(M_e) / PF	BLD-PF(8 M$_e$)	4500	414 000	0.9	8.3	0.5	0.5
	BLD-PF(14 M$_e$)	4500	710 000	0.9	14.2	0.5	0.5
CASE III	BLD-PF(0.1)	4500	710 000	0.9	14.2	0.9	0.1
PI(M_e) / PF(14M_e)	BLD-PF(0.2)	4500	710 000	0.9	14.2	0.8	0.2
	BLD-PF(0.4)	4500	710 000	0.9	14.2	0.6	0.4
	BLD-PF(0.5)	4500	710 000	0.9	14.2	0.5	0.5
	BLD-PF(0.6)	4500	710 000	0.9	14.2	0.4	0.6
	BLD-PF(0.9)	4500	710 000	0.9	14.2	0.1	0.9

Novocontrol Alpha high-resolution frequency analyzer, within the frequency range from 10^{-2} to 10^{7} Hz, and for temperatures in the range from 173.15 to 333.15 K. All samples, before measurement, were placed into an oven under vacuum conditions in order to remove traces of water/solvent. The DS measuring cell consisted of two platinum electrodes (of 20 mm diameter) forming a capacitor. A Teflon spacer was inserted in the sample to keep the distance of the electrodes fixed (≈50 µm). By applying an alternating electric field to the capacitor, the complex dielectric function (ϵ^*) is obtained as a function frequency (ω) and temperature (T). The latter is defined as $\epsilon^* = \epsilon' - i\epsilon''$, where the real part (the dielectric permittivity) refers to the energy that is reversibly stored in the dielectric, and the imaginary part to the dielectric losses. The analysis of the DS resulted in curves was based on the empirical equation of Havriliak and Negami (Equation (1))[25]

$$\varepsilon^*_{HN}(\omega, T) = \varepsilon_\infty(T) + \sum_j \frac{\Delta\varepsilon_j(T)}{\left[1 + (i\omega\tau_{HN_j}(T))^{m_j}\right]^{n_j}} + \frac{\sigma_0(T)}{i\varepsilon_f\omega} \quad (1)$$

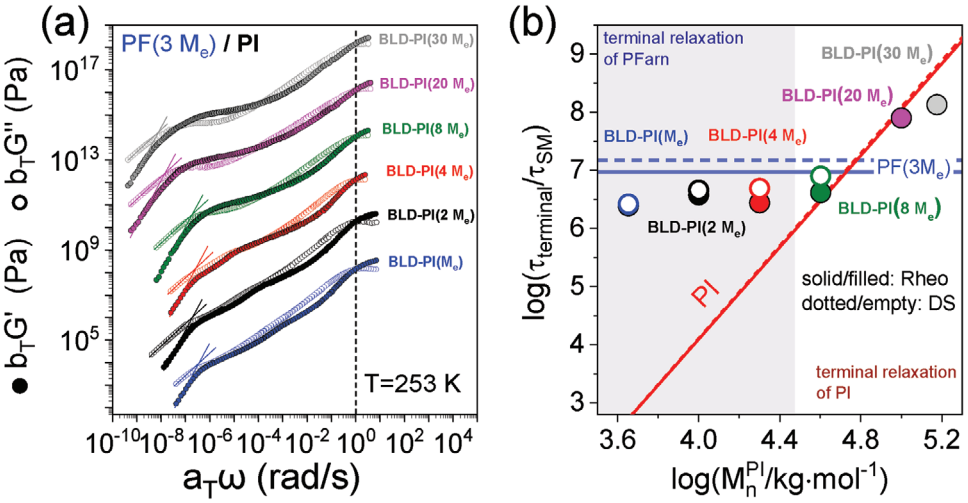

Figure 1. a) Master curves for the storage (filled circles) and loss (open circles) moduli of the symmetric binary blends of PF/PI having a fixed PF molar mass (M_n^{PF} = 129 000 g mol^{-1}) and different PI molar masses: M_e (blue), $2M_e$ (black), $4M_e$ (red), $8M_e$ (green), $20M_e$ (magenta), and $30M_e$ (gray), all at T = 253 K. Master curves are normalized to the segmental relaxation time, τ_{SM}, and are further shifted vertically for clarity. Linear fit with respective slopes 2 and 1 for the storage and loss moduli are shown, characteristic of the terminal relaxation. b) Terminal relaxation times, normalized by the respective segmental times in the binary blends plotted as a function of PI molar mass. Solid lines give the τ_{term}/τ_{SM} for PI (shown in red) and PF (shown in blue) from rheology and corresponding dashed lines from DS. Symbols indicate the normalized τ_{term} from rheology (filled circles) and DS (open circles), respectively. Grey and white areas indicate regimes dominated by PF and PI terminal dynamics.

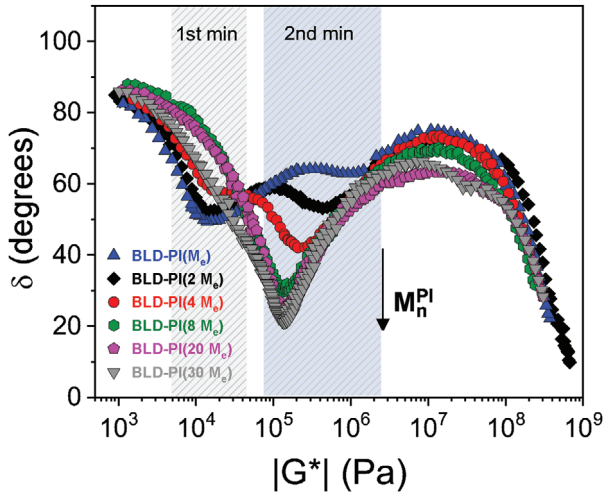

Figure 2. The van Gurp–Palmen plot for the symmetric binary blends of PF/PI shown for different PI molar masses: BLD-PI(M_e) (blue triangles), BLD-PI($2M_e$) (black rhombi), BLD-PI($4M_e$) (red spheres), BLD-PI($8M_e$) (green hexagons), BLD-PI($20M_e$) (magenta pentagons) and BLD-PI($30M_e$) (gray down-triangles). In the first three cases, two weak minima are evident, while in the three latter cases, one strong minimum below 40° indicates the blend plateau modulus.

where $\varepsilon_\infty(T)$ is the high-frequency permittivity, ϵ_f is the permittivity of free space, $\tau_{HN}(T)$ refers to the characteristic relaxation time of this model, $\Delta\varepsilon(T) = \varepsilon_0\ (T) - \varepsilon_\infty(T)$ is the relaxation strength of the process under investigation, m and n are the two shape parameters of the HN equation (with $0 \le m_j, m_j n_j \le 1$), ω ($= 2\pi f = 1\ /\ \tau$) is the angular frequency of the external electric field, and $\sigma_0(T)$ introduces the conductivity contribution. From the τ_{HN} the relaxation times at maximum loss, τ_{max}, were obtained analytically from the HN equation as follows:

$$\tau_{max} = \tau_{HN}\left[sin\left(\frac{\pi m}{2\,(1+n)}\right)\right]^{-1/m}\left[sin\left(\frac{\pi mn}{2\,(1+n)}\right)\right]^{1/m} \quad (2)$$

In the temperature range where two or more relaxation processes contribute to ϵ^*, a summation of HN functions was used, assuming statistical independence in the frequency domain.

3. Results and Discussion

With the binary polyterpene blends of the "bottlebrush PF" and the linear PI we explore three cases. In the first section (Case I) we study the effect of PI molar mass on tube dilation by employing several symmetric PF/PI blends having an entangled PF (with $Z_{PF} = 2.6$), and different PIs (molar masses from $Z_{PI} = 0.9$ to 30). More efficient tube dilation effects can be obtained by exploring the effect of PF molar mass ($Z_{PF} = 2.6$ to 14.2) in blends with a fixed PI ($Z_{PI} = 0.9$) (Case II). In the last section (Case III) we employ the most efficient supersoft polymer melt (with $Z_{PF} = 14.2$, and $Z_{PI} = 0.9$) and explore the effect of blend composition.

3.1. CASE I: Effect of PI Molar Mass

In the first case, we explore the effect of PI molar mass by preparing several symmetric PF/PI blends having a fixed PF molar mass ($Z_{PF} = 2.6$) and different PI molar masses from unentangled ($Z_{PI} = 0.9$) to well-entangled ($Z_{PI} = 30$) (**Table 1**). The master curves of the blends are shown in **Figure 1**. They were constructed at the same reference temperature ($T = 253$ K) and further normalized to the segmental relaxation time. A clear plateau is observed only in cases where the PI molar mass is above $\approx 8M_e$. The terminal relaxation in the blends shows a distinct dependence on PI molar mass (Figure 1b). When the PI molar mass is below $\approx 8M_e$ the terminal relaxation follows the corresponding PF relaxation (where $Z_{PF} = 2.6$). On the other hand, for PI molar masses above $8M_e$ ($Z_{PI} = 7.8$) the terminal relaxation is dictated by the longer PI chains. In this respect, the blend BLD-PI($8M_e$) lies at the borderline between PF- and PI-dominated terminal regimes. Figure 1b contains, in addition to the terminal relaxation from rheology, the longest normal mode as obtained from DS, for comparison. The results are in good agreement, as expected from the low polarity of PI and PF.

More informative with respect to the viscoelastic properties of the blends, and in particular regarding the applicability of time-temperature superposition, is the van Gurp–Palmen plot (vGP)[26,27] of the phase angle δ versus logG^* ($|G^*| = (G'(\omega)^2 + G''(\omega)^2)^{1/2}$). In a material following tTs, prior to any shift, all isothermal data in the vGP plot overlap in a single master curve. Starting from the terminal regime (where $\delta = 90^0$) and moving across the modulus scale, the modulus first decreases to a minimum value that is characteristic of the plateau modulus, G_N^0. The more entangled the polymer the deeper is the minimum. Subsequently, δ increases, goes through a maximum, and decreases again to another minimum, in the vicinity of the glass "transition" ($|G^*| = 10^9$ Pa). In the blends, one can observe several distinct features. First, tTs is only partially obeyed, especially on approaching the liquid-to-glass temperature. The reason is that PF has a lower T_g than PI (T_g(PF) ≈200 K and T_g(PI) ≈207 K).[9,10] In the blends, there exists a single, albeit broad T_g giving rise to the lack of a perfect superposition. Nevertheless, to a good approximation, the blends can be regarded as *isofrictional*. Second, in blends where the PI molar mass is higher than $\approx 8M_e$, a clear minimum in δ is observed (with values in the range $20^0 < \delta < 30^0$) at $|G^*| = 10^5$ Pa giving the plateau modulus. In blends where M(PI)< $8M_e$, two shallow minima are observed suggestive of two quasi-elastic regimes. The first minimum in δ, $G^*_{\delta^1_{min}}$, between the terminal relaxation and the plateau modulus associates with the relaxation of the PF ($3M_e$) chains in the blend. As for the second minimum in δ, $G^*_{\delta^2_{min}}$, it was shown that it associates with the steady-state recoverable compliance, as it shifts with decreasing PI molar mass.[27] (**Figure 2**)

We can further explore the plateau modulus and obtain respective values for the entanglement molar mass, M_e, packing length, p, and tube diameter, d_T, using $M_e = \frac{4}{5}\frac{\rho RT}{G_N^0}$, where ρ is the mass density ($\rho_{PI} = 0.91$ g cm^{-3};[28] $\rho_{PF} = 0.90$ g·cm^{-3} [10]), $M_e = 218\rho p^3$, and $d_T = 19p$.[28] The result is shown in **Figure 3**. We emphasize here, that the interpretation of the value of $|G^*|$ at the first and second (main) δ_{min} as corresponding to the plateau modulus is accurate only for the three blends with the strong single δ_{min}. For it is only in the latter case that the $G^*_{\delta^2_{min}}$ value corresponds exactly to the plateau modulus. Nevertheless, we calculate these quantities even for blends with M(PI)< $8M_e$ to explore some trends.

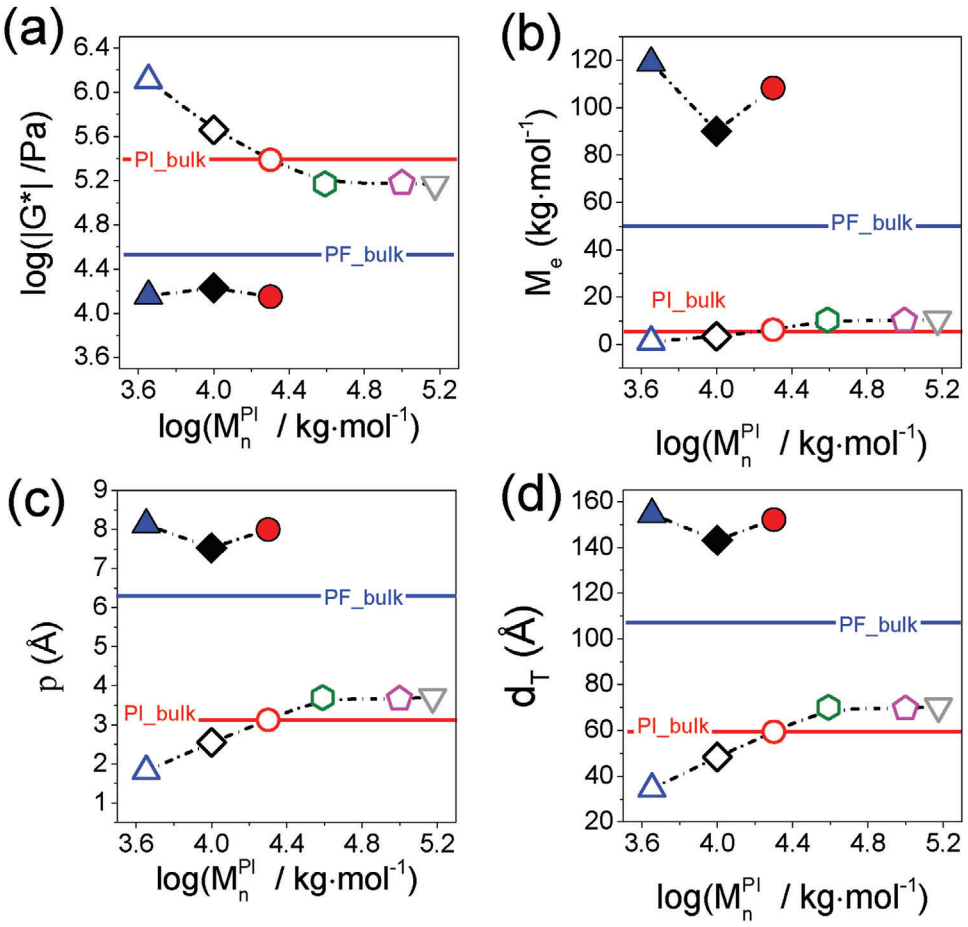

Figure 3. Viscoelastic properties of the symmetric binary blends PF/PI having a fixed PF molar mass (M_n^{PF} = 129 000 g mol^{-1}) and different PI molar masses. a) The absolute value of the complex shear modulus as a function of PI molar mass. Filled symbols correspond to the first minimum in the van Gurp-Palmen plot, while open symbols correspond to the second minimum. b) Entanglement molar mass is plotted as a function of the PI molar mass. c) Packing length over the molar mass of the PI component. d) Tube diameter as a function of PI molar mass in the blend. Red and blue solid lines correspond to well-entangled homopolymers of PI and PF, respectively.

The value of the $G^*_{\delta^1_{min}}$ corresponding to the terminal relaxation of PF in the blends with M(PI)< 8M_e results to a higher M_e, p, and d_T values with respect to the PF homopolymer. This is one aspect of dynamic tube dilation in blends of long/short chains with identical chemistry that has been explored earlier.[17–24] Effectively, the lower molar mass PI acts as a solvent to the PF component, alleviating the constraints and increasing the tube diameter of PF. More efficient tube dilation effects can be obtained by exploring the effect of PF molar mass in blends with a fixed PI molar mass (Case II, below).

3.2. CASE II: Effect of PF Molar Mass

Here we explore the viscoelastic properties in three blends having a fixed PI molar mass (M_e; Z_{PI} = 0.9), and PF with increasing molar mass (from Z_{PF} = 2.6 to 14.2). The master curves for the blends are compared with the pure components in **Figure 4**. For the BLD-PI(M_e)-PF(3M_e), the rubbery plateau is not pronounced, and the terminal relaxation speeds up as compared to the PF homopolymer (Figure 4a). In the other extreme, the BLD-PI(M_e)-PF(14M_e) blend, the rubbery plateau is clearly evident, but the plateau modulus is decreased nearly by an order of magnitude (Figure 4c). Evidently, blending high molar mass PF with short PI chains results in an efficient dynamic tube dilation (Figure 4d), giving rise to super-soft polymer melts.

How effective is the obtained supersoft polymer melt? To address this question, we explore the details of the vGP plot (**Figure 5**). The plot reveals one sharp minimum that is very distinct in the BLD-PF(14M_e) (δ_{min}~20^0), and in BLD-PF(8M_e) (δ_{min}~36^0), but much less distinct in BLD-PF(3M_e) (δ_{min}~50^0). The value of modulus at the minimum shifts from $|G^*| = 3.4 \times 10^4$ Pa in PF(14M_e) homopolymer, to $|G^*| = 7.3 \times 10^3$ Pa in the BLD-PF(14M_e), i.e., a sixfold decrease in the plateau modulus. This again suggests that efficient supersoft polymers can be designed by mixing a well-entangled bottlebrush polymer (PF component) with a low molar mass linear (PI component) polymer.

The effect of increasing PF molar mass on M_e, the packing length, p, and the tube diameter, d_T, are shown in **Figure 6**. The figure shows an increasing entanglement molar mass (Figure 6b), packing length (Figure 6c), and tube diameter (Figure 6d) with increasing PF molar mass in the blends.

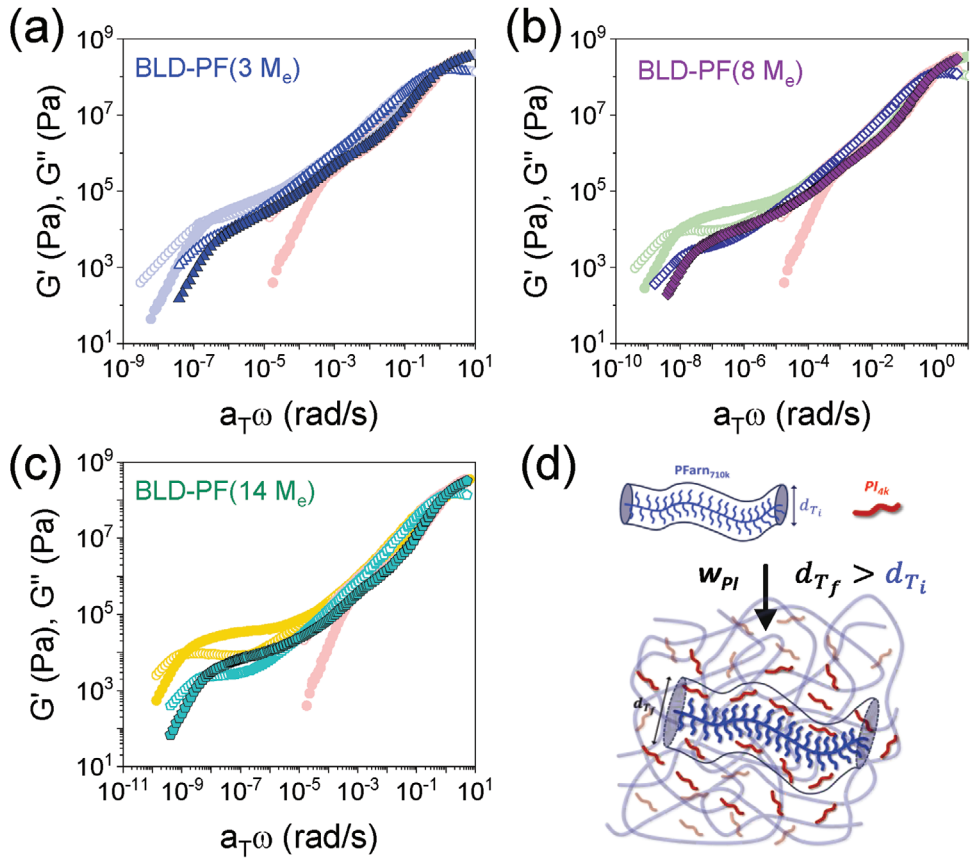

Figure 4. Master curves of the storage (filled symbols) and loss (open symbols) moduli for the bulk components (pale colors) and the PI(M_e) – PF blends for the three different cases of a) BLD-PF(3M_e), b) BLD-PF(8M_e) and c) BLD-PF(14M_e). In all cases, data are normalized to their segmental relaxation time. d) Graphical representation of the tube dilation effect, where the low molar mass PI acts as a solvent for the well-entangled PF component.

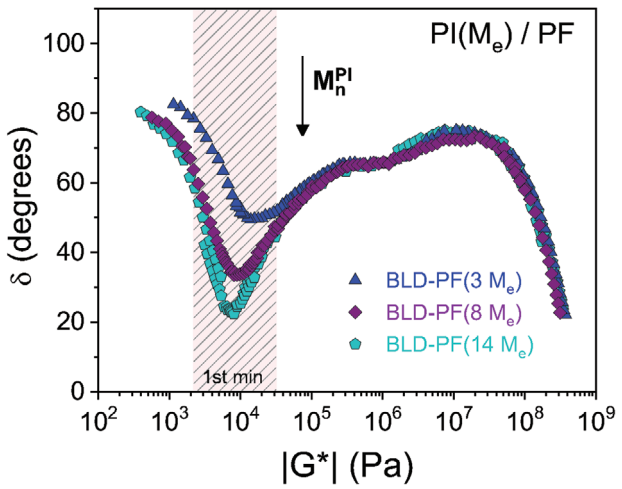

Figure 5. Van Gurp–Palmen plot for the three symmetric binary blends PF/PI having a fixed PI molar mass ($M_n^{PI} = 4500$ g mol^{-1}) and different PF molar masses: BLD-PF(3M_e) (blue), BLD-PF(8M_e) (purple) and BLD-PF(14M_e) (light green). One strong minimum is evident in the latter two cases, together with a barely distinguishable second minimum, corresponding to the chain relaxation of the low molar mass constituent, PI(M_e). By increasing the molar mass of PF, $|G^*|$ moves to lower values, adapting properties similar to those of supersoft polymers.

Interestingly, the PF tube diameter is nearly doubled by blending PF(14M_e) with a low molar mass PI(M_e) that acts as a diluent. In the next section, we employ the most efficient supersoft polymer blend and explore the effect of blend composition on further controlling the plateau modulus.

3.3. CASE III: Effect of Blend Composition on Tube Dilation

Can we make better supersoft melts by controlling the bottlebrush/linear polymer blend composition? To this end, we employ the well-entangled PF(14M_e) and prepare blends with a low molar mass PI(M_e) at different ratios. **Figure 7** compiles the respective mastercurves for the storage modulus in the homopolymers and their blends. The results show a decreasing rubbery plateau with increasing PI content. In the inset, the normalized terminal relaxation times, are plotted as a function of the PF weight fraction in a double logarithmic representation. The results reveal a dependence as $\tau_{term} \sim w_{PF}^{1.5}$.

To explore further the details of the viscoelastic properties in the blends we discuss the vGP plot with the help of **Figure 8a**. Two minima are evident in some cases; the first minimum corresponds to the transition from the terminal relaxation of the blend to the rubbery plateau, whereas the second (shallow) minimum corresponds to the chain relaxation of the low molar

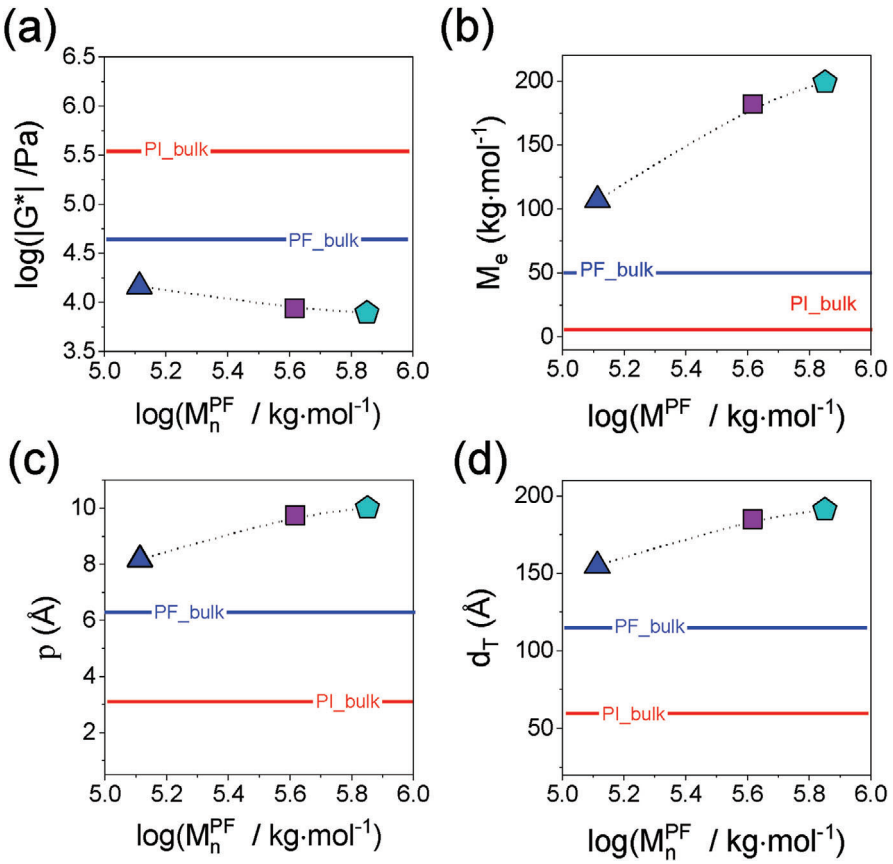

Figure 6. a) Absolute value of the complex shear modulus as a function of PF molar mass for the three symmetric binary blends PF / PI having a fixed PI molar mass (M_n^{PI} = 4500 g mol^{-1}) and different PF molar masses: BLD-PF(3M_e) (blue triangle), BLD-PF(8M_e) (purple square) and BLD-PF(14M_e) (light green pentagon). For the extreme case of PF(14M_e)-PI(M_e) the plateau value is lower than 10^4 Pa, exhibiting properties similar to supersoft polymer melts (see text). b) Entanglement molar mass, c) packing length, and d) tube diameter plotted as a function of the PF molar mass in the blends. Red and blue solid lines give respective values for well entangled PI and PF homopolymers.

mass component (PI). The first minimum in δ, $G^*_{\delta^1_{min}}$, is deep in the cases of $w_{PF} \geq 0.4$ and becomes shallow for $w_{PF} \leq 0.2$. As shown in Figure 8b, $1/G^*_{\delta^1_{min}} \sim w_{PF}^{-1.75}$, a somewhat weaker dependence than the one reported for blends of linear polymers (e.g., polystyrene). [27]

The extracted parameters from the absolute value of the complex shear modulus at $G^*_{\delta^1_{min}}$, i.e., the entanglement molar mass, the packing length, and the tube diameter are plotted in **Figure 9** as a function of the weight fraction of PF in the blends. It is evident that the value of $|G^*|$ decreases with decreasing PF fraction in a nonlinear way. Data obtained for the M_e, p, and d_T in the case of the two blends with $w_{PF} \leq 0.2$ are shown in faint color, since a clear rubbery plateau is not observed in this case. For the remaining blends, results show significant tube dilation with increasing PI content. In the case of $w_{PF} = 0.4$ the entanglement molar mass increases to ≈300 kg mol^{-1} (from 50 kg mol^{-1} in PF), the packing length to ≈11.5 Å (from 6.3 Å in PF), and the tube diameter to 220 Å (from 116 Å in PF).[9,10]

The efficiency in tube dilation by chain architecture can be compared for different PI topologies (linear/linear, linear/star, and linear/bottlebrush) by plotting the dilated tube diameter in the blends reduced by the respective value in undiluted long

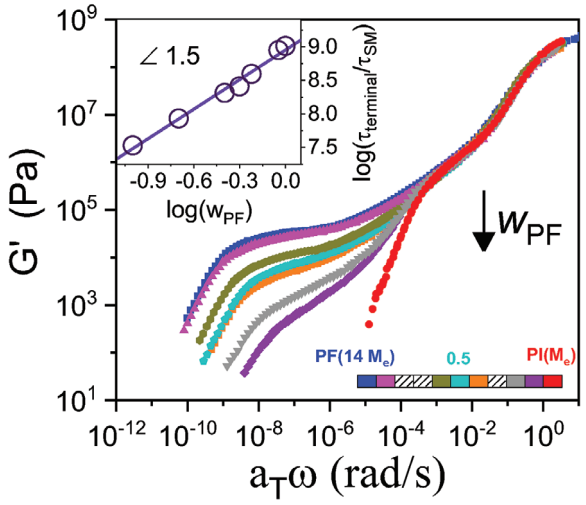

Figure 7. Mastercurves of the storage moduli (G') normalized at the segmental relaxation times, for blends with various blend compositions. A significant reduction in the plateau modulus is evident. In the inset, the terminal relaxation times, normalized to the segmental relaxation times, are plotted as a function of the PF weight fraction in a double logarithmic plot. A line with a slope of 1.5 is shown.

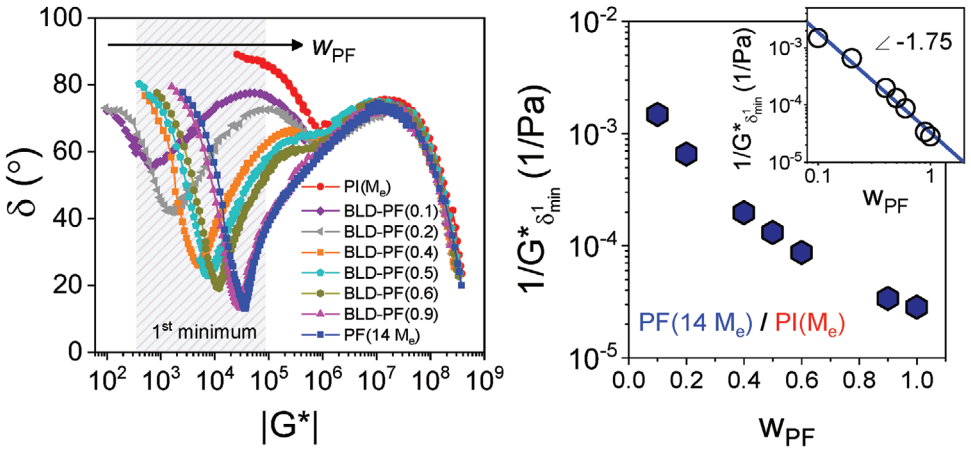

Figure 8. (Left) van Gurp–Palmen plot for the blends with different PF weight fractions: BLD-PF(0.1) (purple), BLD-PF(0.2) (gray), BLD-PF(0.4) (orange), BLD-PF(0.5) (light green), BLD-PF(0.6) (olive), BLD-PF(0.9) (magenta), PI(M_e) (red), PF(14M_e) (blue). (Right) The inverse of $|G^*|$ at the first δ minimum is plotted over the weight fraction of the high molar mass component, w_{PF}. In the inset, the same data are shown in a double logarithmic representation. The blue solid line indicates that $1/G^*_{\delta^1_{min}}$ varies with w_{PF} in the power of −1.75.

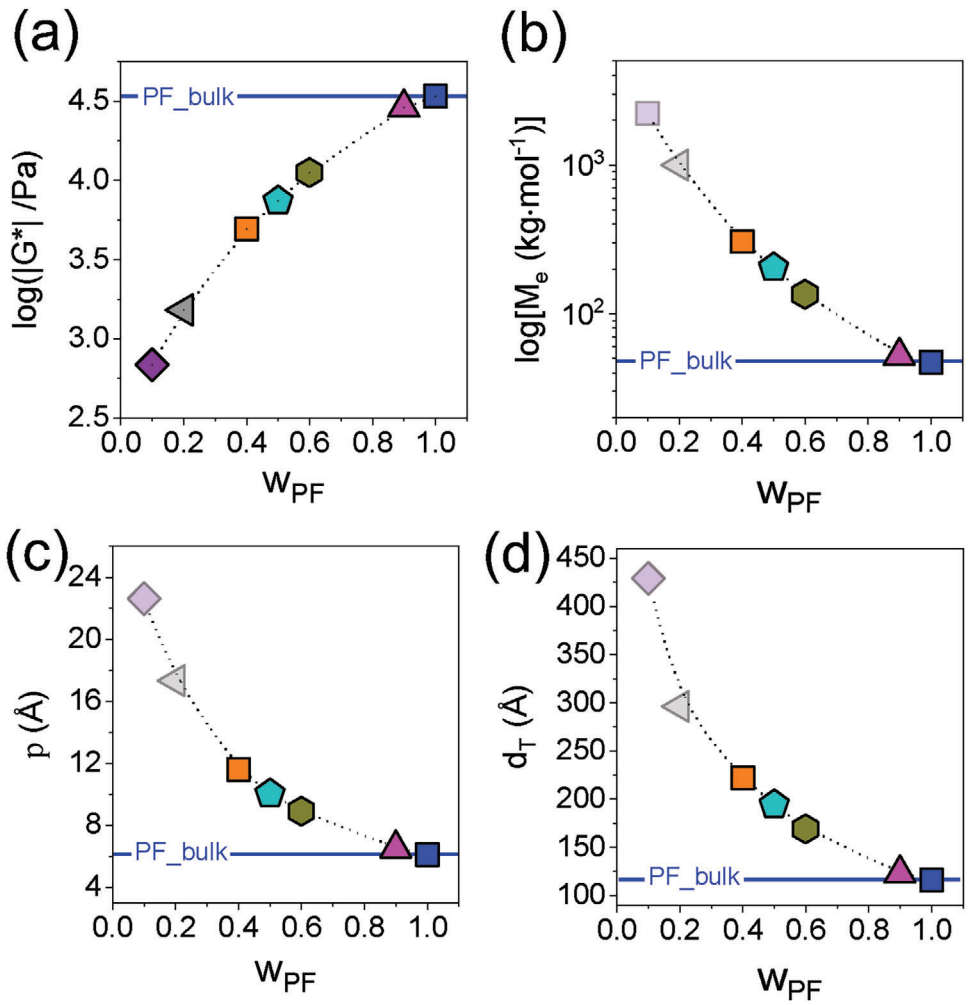

Figure 9. a) Absolute value of the complex shear modulus at $G^*_{\delta^1_{min}}$ as a function of the weight fraction of the PF in the blends. Dependence of b) the entanglement molar mass, c) the packing length, and d) the tube diameter, as a function of PF weight fraction. The dotted line is a guide for the eye. Blue solid line indicates the corresponding values for the PF(14M_e) homopolymer.

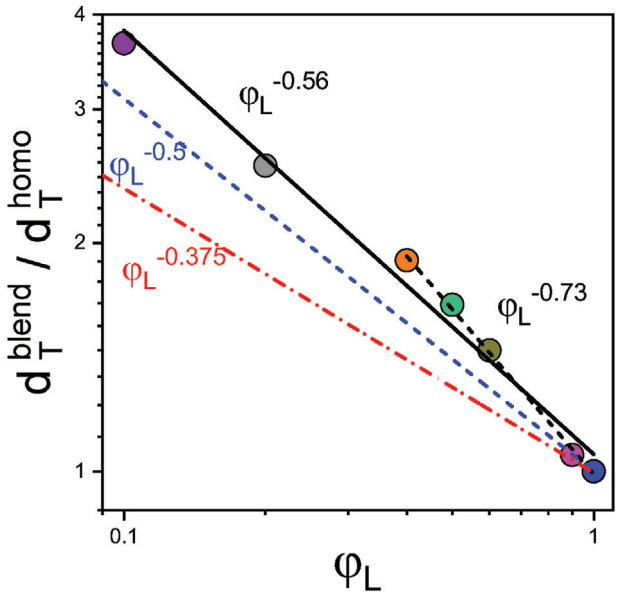

Figure 10. Architecture-induced tube dilation. Tube diameter in blends relative to the respective homopolymers for a) linear PI blends PI($16M_e$)/PI($2.4M_e$) shown with the red dash-dotted line, b) blends of the same linear PI($16M_e$) with PI stars,[24] shown with the dashed blue line), and c) the present bottlebrush/linear PF/PI blends shown with the black line.

homopolymer, as a function of the volume fraction of long chains, φ_L, in **Figure 10**. The figure depicts tube dilation in linear/linear PI blends scaling as $\varphi_L^{-0.5}$, and in linear/star PI blends scaling as $\varphi_L^{-0.375}$.[24] This should be contrasted with the present PF/PI (bottlebrush/linear) blends where tube dilation scales as $\varphi_L^{-0.56}$. Employing only blends where the rubbery plateau is more evident (e.g., ignoring the data points with $w_{PF} \leq 0.2$), it provides an even steeper dependence, e.g. scaling as $\varphi_L^{-0.73}$. Overall, the results show that among the different topologies examined, blends comprising bottlebrush/linear chains are more effective in the process of tube dilation resulting in supersoft polymer melts. The explanation for this key observation is the low rubbery plateau value of the bottlebrush polymer. Further crosslinking of the longer chains will result in supersoft elastomers.

4. Conclusion

Bottlebrush polymers are solvent-free melts with a plateau modulus as low as 1 kPa, a value typically found in swollen networks and required to match soft biological tissues. We employed binary blends of polyterpenes comprising linear (*cis*-1,4-PI) and bottlebrush (*cis*-1,4-PF) topologies to explore the possibility of further reducing the – already low–plateau modulus of PF ($G_N^0 \sim 3.5 \times 10^4$ Pa) by tube dilation. The new *athermal* and largely *isofrictional* PF/PI blends constitute a new class of supersoft polymer melts with plateau moduli in the range from 10 to 1 kPa. The efficiency in tube dilation relates to polymer architecture; we deduce that blends of polyterpenes are more effective than long/short PI blends, as well as from linear/star PI blends, i.e., blends with identical chemistry. This opens a new area, where bottlebrush/linear *athermal* polymer blends can be employed as a means to adjust the elasticity and flow behavior in polymer melts and thereby lead to supersoft elastomer materials after crosslinking.

Supporting Information

Supporting Information is available from the Wiley Online Library or from the author.

Acknowledgements

This work was supported by the program "PERIFEREIAKI ARISTEIA" (Regional Excellence) co-financed by the European Union and the Hellenic Republic Ministry of Development and Investments under NSRF 2014–2020 (Region of Epirus, call 111).

Open access funding enabled and organized by Projekt DEAL.

Conflict of Interest

The authors declare no conflict of interest.

Data Availability Statement

The data that support the findings of this study are available from the corresponding author upon reasonable request.

Keywords

bottlebrush polymers, polymer blends, polyterpenes, supersoft polymers, tube dilation

Received: July 5, 2024
Published online: August 26, 2024

[1] Y.-C. Fung, *Biomechanics: Mechanical Properties of Living Tissues*, Springer, **2013**.
[2] M. A. Meyers, P.-Y. Chen, A. Y.-M. Lin, Y. Seki, *Prog. Mater. Sci.* **2008**, *53*, 1.
[3] W. F. M. Daniel, J. Burdyńska, M. Vatankhan-Varnoosfaderani, K. Matyjaszewski, J. Paturej, M. Rubinstein, A. V. Dobrynin, S. S. Sheiko, *Nat. Mater.* **2016**, *15*, 183.
[4] H. Liang, B. J. Morgan, G. Xie, M. R. Martinez, E. B. Zhulina, K. Matyjaszewski, S. S. Sheiko, A. V. Dobrynin, *Macromolecules* **2018**, *51*, 10028.
[5] S. S. Sheiko, A. V. Dobrynin, *Macromolecules* **2019**, *52*, 7531.
[6] Z. Li, M. Tang, S. Liang, M. Zhang, G. M. Biesold, Y. He, S.-M. Hao, W. Choi, Y. Liu, J. Peng, Z. Lin, *Prog. Polym. Sci.* **2021**, *116*, 101387.
[7] T. A. Kavassalis, J. Noolandi, *Macromolecules* **1989**, *22*, 2709.
[8] T. Pakula, Y. Zhang, K. Matyjaszewski, H. Lee, H. Boerner, S. Qin, G. C. Berry, *Polymer* **2006**, *47*, 7198.
[9] I. Tzourtzouklis, C. Hahn, H. Frey, G. Floudas, *Macromolecules* **2022**, *55*, 8766.
[10] C. Iacob, T. Yoo, J. Runt, *Macromolecules* **2018**, *51*, 4917.
[11] C. Tang, C. Y. Ryu, *Sustainable Polymers from Biomass*, 1st ed. Wiley-VCH, Weinheim **2017**.
[12] C. Wahlen, H. Frey, *Macromolecules* **2021**, *54*, 7323.

[13] C. Wahlen, J. Blankenburg, P. von Tiedemann, J. Ewald, P. Sajkiewicz, A. H. E. Müller, G. Floudas, H. Frey, *Macromolecules* **2020**, *53*, 10397.
[14] C. Wahlen, J. Bareuther, J. Blankenburg, M. Appold, L. Shaw, A. H. E. Müller, G. Floudas, L. R. Hutchings, M. Gallei, H. Frey, *Macromolecules* **2020**, *53*, 10397.
[15] R. Everaers, S. K. Sukumaran, G. S. Grest, C. Svaneborg, A. Sivasubramanian, K. Kremer, *Science* **2004**, *303*, 823.
[16] M. Doi, S. F. Edwards, *The Theory of Polymer Dynamics*, Oxford University Press, Oxford **1988**.
[17] G. Marucci, *J. Polym. Sci., Part B: Polym. Phys.* **1985**, *23*, 159.
[18] M. J. Struglinski, W. W. Graessley, L. J. Fetters, *Macromolecules* **1988**, *21*, 783.
[19] M. Doi, W. W. Graessley, E. Helfand, D. S. Pearson, *Macromolecules* **1900**, *20*, 1987.
[20] J. L. Viovy, M. Rubinstein, R. H. Colby, *Macromolecules* **1991**, *24*, 3587.
[21] J. H. Lee, L. J. Fetters, L. A. Archer, A. F. Halasa, *Macromolecules* **2005**, *38*, 3917.
[22] E. van Ruymbeke, Y. Masubuchi, H. Watanabe, *Macromolecules* **2012**, *45*, 2085.
[23] E. van Ruymbeke, V. Shchetnikava, Y. Matsumiya, H. Watanabe, *Macromolecules* **2014**, *47*, 7653.
[24] P. Malo de Molina, A. Alegria, J. Allgaier, M. Kruteva, I. Hoffmann, S. Prévost, M. Monkenbusch, D. Richter, A. Arbe, J. Colmenero, *Macromolecules* **2020**, *53*, 5919.
[25] F. Kremer, A. Schönhals, *Broadband Dielectric Spectroscopy*, Springer, Berlin **2002**
[26] M. van Gurp, J. Palmen, *Rheology Bulletin* **1998**, *67*, 5.
[27] Z. Qian, G. B. McKenna, *Polymer* **2018**, *155*, 208.
[28] L. J. Fetters, D. J. Lohse, W. W. Graessley, *J. Polym. Sci. Part B: Polym. Phys.* **1999**, *37*, 1023.

